Plasma Profile Recovery by Function Parameterisation

P.J. Mc Carthy* and M.C. Sexton[1]

IPP 5/12 November 1986

MAX-PLANCK-INSTITUT FÜR PLASMAPHYSIK

8046 GARCHING BEI MÜNCHEN

MAX-PLANCK-INSTITUT FÜR PLASMAPHYSIK

GARCHING BEI MÜNCHEN

Plasma Profile Recovery by Function Parameterisation

P.J. Mc Carthy* and M.C. Sexton[1]

IPP 5/12 November 1986

*On attachment from University College, Cork, Ireland

[1]University College, Cork, Ireland

Die nachstehende Arbeit wurde im Rahmen des Vertrages zwischen dem Max-Planck-Institut für Plasmaphysik und der Europäischen Atomgemeinschaft über die Zusammenarbeit auf dem Gebiete der Plasmaphysik durchgeführt.

PLASMA PROFILE RECOVERY BY FUNCTION PARAMETERISATION

P.J. Mc Carthy* and M.C. Sexton[1]

*On attachment from University College, Cork, Ireland
[1]University College, Cork, Ireland

Abstract

The use of Function Parameterisation for the recovery of plasma profiles as a function of flux surface area from spatial point data directly combined with external magnetic measurements is demonstrated in the case of ASDEX electron temperature and density profiles. The extrapolated temperature on the magnetic axis is shown to be more reliable than that obtained from a conventional fitting procedure.

1. INTRODUCTION

The processing of plasma diagnostic raw data frequently involves the iterative fitting of a given physical model to obtain best estimates of various intrinsic plasma parameters of interest. The complexity of the model and the corresponding time requirement may render the task feasible only in the context of off-line analysis. A separate problem may exist where a large number of raw measurements are analysed: If some data are highly correlated, the analysis will be prone to numerical instabilities unless steps are taken to detect such inter-dependencies.

Despite the large number of inherent degrees of freedom in a plasma, the behaviour of many physically interesting quantities in a given experimental configuration seems to be characterised by a relatively modest dimensionality. A statistical analysis of the relationship between desired plasma parameters and the diagnostic raw measurements, with the goal of a more efficient and rapid method of recovering the former from the latter, accordingly suggests itself.

Such an approach to the recovery of physical parameters from raw data, named Function Parameterisation (FP) by its developer, was pioneered by H. Wind for the purpose of momentum determination from spark chamber data [1],[2]. The technique may be broadly summarised by the following three-stage process:

(a) A large database of simulated experimental data, including both raw measurements and desired physical information, is constructed using the actual experimental and diagnostic configuration together with a realistic model of the possible physical states of the system.

(b) Near-linear dependencies in the simulated raw measurements are screened out by a suitable statistical technique.

(c) The simulated physical parameters are regressed against simple functions of the statistically optimised raw data. Once evaluated, these functions may be repeatedly used as a fast and efficient means of recovering the same physical parameters from real raw measurements.

A succinct mathematical description is contained in a recent paper by Braams *et al.* [3] in which, following an earlier proposal [4], the first application in the context of controlled fusion research is reported. In that work, FP is applied to the rapid determination of characteristic MHD equilibrium parameters for a divertor tokamak plasma in the ASDEX experiment. The feasibility of controlling the evolution of the discharge in real-time using FP-calculated quantities is indicated. We now extend this work to include internal plasma measurements of electron temperature and density.

These spatial measurements are combined directly with the magnetic measurements to yield electron temperature or density profiles as a function of flux surface area (or radius) as output. It is shown that satisfactory recovered profiles are obtained in a time compatible with the provision of profile information for real-time control purposes. The fixed geometry of the internal measurements used in this application is such that for discharges with comparatively large values of $\beta_p + l_i/2$, the magnetic axis is removed from the spatial profile raw data by up to one third of the minor radius. Comparison of the necessarily extrapolated axis temperatures with those of a separate diagnostic, which can be positioned to directly measure the temperature on axis, shows that FP-predicted axis temperatures are significantly more reliable than those obtained from a conventional fitting procedure.

2. Database Preparation

2.1 Raw Measurements. The following ASDEX external magnetic raw measurements are used in the present FP application (see Fig. 1): Three differential poloidal flux measurements, four poloidal field measurements, the current through the principal multipole shaping coil and the multipole shunt current measured as signal MPIS in ASDEX diagnostic # 3. All nine measurements are scaled to unit plasma current.

The diagnostic providing the spatial profile raw data used in the present work is the Nd:YAG 60 Hz 16-channel repeating laser system for Thompson scattering - determined electron temperatures and densities [5],[6]. The positions of the magnetic and profile measurements in relation to the plasma column are shown in Fig. 1.

2.2 Magnetic Data. The Garching Equilibrium Code (forward version) [7] was used to generate *c.* 5000 divertor equilibria in which the free parameters in the code were varied to adequately cover ASDEX operating conditions up to the spring 1986 shutdown. A dataset was stored on disk for each equilibrium consisting of:
(a) The nine external magnetic measurements described in the preceding subsection.
(b) The following physical information: The cross-sectional area and poloidal flux of the flux surface passing through each of the fixed positions of the sixteen Thompson scattering channels. The set of plasma parameters (the magnetic and geometric centre of the plasma column, the plasma area and $\beta_p + l_i/2$ are of particular interest in this application) whose recovery was the object of the application described in [3].

2.3 Profile Data. The following procedure was employed to generate a database of flux surface profiles: Some 2000 electron temperature and density profiles, with error bars as returned by the ASDEX LASER program, were assembled from 25 shots spanning the time period spring 1985 to spring 1986 and chosen to cover a wide variety of discharges. Using the existing FP code (see [3] section 3.6) to calculate the plasma area and the co-ordinates of the magnetic axis and geometric centre for each spectrum, it was then possible to calculate the normalised flux surface radii through each spatial point using the model of nested horizontally shifted flux circles which is adequate to describe the magnetic structure of ASDEX equilibria. To ensure a vanishing slope on the magnetic axis, The 15 transformed raw data points (because it is more often than not submerged in noise, the 16^{th} channel at $z = -39.5$ cm was not considered) were reflected about the $\rho = 0$ axis giving a 30 - point symmetry spectrum. To enable extrapolation of the fitted profile to the plasma edge in all cases, two pseudo points with values of half the 15^{th} channel but with low weightings (200% error) were added

at $\rho = 1.0$ and $\rho = -1.0$ (where ρ is the normalised flux surface radius). The complete 32 - point spectrum, with error bars, was then submitted to the weighted least squares B-spline Nag routine E02BAF with knots at ρ values of -0.5, -0.25, 0.25 and 0.5. This knot grouping, decided upon after some experimentation, provides only four independent spline coefficients per spectrum on account of the imposed symmetry of the data. Given the quality of the raw data, four independent parameters seems sufficient to describe the various profile types encountered, including pronounced shoulders and central hollows.

3. Statistical Analysis of the Database

3.1 Construction of Parameter and Raw Measurement Matrices. The database whose generation has just been described may now be repeatedly analysed using various statistical techniques. The criterion by which a chosen approach is to be judged is the closeness of agreement between the exact and FP - recovered plasma parameters. The scheme adopted for the present work is now described:

A matrix of simulated raw measurements is constructed using both randomly selected magnetic data sets and randomly selected spline profiles in the following fashion: The selected profile is evaluated at each of the 15 spatial channels using a circular equivalent or geometric mean - type flux surface radius defined to be the square root of the cross-sectional area of the flux surface through each channel normalised to the plasma area (recall that these quantities are stored in the magnetic data set) as the ρ value for that channel; i.e.

$$P(z_i) = S\left(\sqrt{\frac{A_i}{A_P}}\right), \quad i = 1, 15 \tag{1}$$

where $P = T_e$ or $P = n_e$ and S is the selected spline profile. To these simulated spatial measurements are added the nine magnetic measurements described in section 2, giving a row of 24 raw measurements for each equilibrium. A matrix of *c.* 3000 rows (the cases of upper and lower null points were treated separately, see [3] section 3.) is assembled in this manner. For each row of raw measurements, a corresponding set of the plasma parameters to be recovered is also stored yielding a 3000 x NP parameter matrix, where NP is the number of parameters. The parameters recovered in this work are detailed in subsection 3.3 below.

3.2 Principal Component Analysis. Each column in the 3000 x 24 raw measurements matrix (consisting of the values taken by a particular raw measurement over the 3000 equilibria) is next scaled to zero mean and unit variance. The 24 x 24 correlation matrix is computed and passed to the Nag routine F02ABF for diagonalisation. This so-called Principal Component Analysis (PCA) [8],[3] yields 24 orthogonal linear combinations of the measurements with corresponding eigenvalues. If the eigenvectors are ordered by eigenvalue magnitude, the resolution of a measurement vector along the n^{th} eigenvector constitutes its n^{th} *principal component* (*p.c.*), though for convenience the term may be applied to the eigenvector itself as well. It should be noted that magnetic and spatial profile information is now coupled together since each *p.c.* has

contributions from all 24 raw measurements. For the case $z_{axis} \leq 0.0$, the following ordered sequence of eigenvalues was obtained: 14.4, 4.03, 1.87, 1.18, 1.03, .935, .315, .109, .0363, .0190, .0158, $6.12 \cdot 10^{-3}$, $4.73 \cdot 10^{-3}$, $1.77 \cdot 10^{-3}$, ... , $2.10 \cdot 10^{-10}$. The $z_{axis} \geq 0.0$ analysis yielded somewhat different results because the distribution of the 15 channels (at approximately 4 cm intervals from $z = 20$ cm to $z = -35$ cm; see Table I) render the profile data up-down asymmetric. Since each scaled raw measurement column has unit variance, the sum of the eigenvalues is also 24. However, the individual eigenvalues vary over 11 orders of magnitude and so the combinations of the measurements corresponding to the smaller values can be regarded effectively as linear dependencies. Such *p.c.*'s , though they may be very useful in detecting erroneous signals (in cases where they stray significantly from their expected values), are, nevertheless, by their nature powerless to describe the variation of any physical quantity. Their elimination from the subsequent regression has the dual advantages of a lower dimensional, more tractable problem and, more significantly, the elimination of near linear dependencies in the raw measurements (see [9], ch. 8). The cut-off point for eigenvector retention is a matter of choice, though comparison of eigenvalue magnitude with expected experimental noise levels provides a useful guideline (for various cut-off criteria, see [9], ch. 7 and [10], ch. 6). After some trial and error, the 11 most significant *p.c.*'s were retained for the subsequent FP regression. The 13 discarded *p.c.*'s comprise less than 0.1% of the total variance, but this rather conservative retention level is seen to be justified by a further pruning procedure described in the next subsection.

3.3 Function Parameterisation. The central part of the FP process consists of the regression of desired physical parameters against simple functions of the leading *p.c.*'s . The chosen approach is to represent the plasma parameters as polynomial combinations of the selected *p.c.*'s . Solely linear *p.c.* combinations were found to be, in general, inadequate. The polynomial degree required for optimal representation is a matter of experimentation. Trials with cubic and quartic combinations of the 11 retained *p.c.*'s showed no justifiable gain in accuracy over the quadratic model for the considerably increased computation involved. The present work, therefore, represents the desired physical parameters as no more than quadratic polynomials in *p.c.* combinations of the raw data. Scrutiny of the 66 possible quadratic combinations of the 11 *p.c.*'s using eigenvalue magnitude as a selection criterion (see [3] section 3) resulted in the retention of the 39 most significant terms which, in combination with the 11 linear terms (plus a column set to 1.0 which is required by the regression routine to produce a constant coefficient), comprise the 3000 row x 51 column independent (or basis) variable regression matrix. Each column in the parameter matrix is separately

regressed against this matrix using the multilinear regression Nag routine G02CJF. Several avenues for profile retrieval were explored, including the recovery of Bessel- or Legendre-type moments. The most satisfactory method so far apparent is direct point-by-point evaluation of the profile as a function of normalised flux surface radius. To this end, the dependent variables were chosen to be the electron temperature or density evaluated at each of 21 equally spaced ρ values ranging from 1.0 (the plasma edge) to 0.0 (the magnetic axis) in increments of $\delta(\rho) = 0.05$. The Shafranov parameter, $\beta_p + l_i/2$, was also included in the profile regression for the purposes of FP error bar calculation (see end of following subsection). A substantial reduction in the number of FP coefficients is now achieved for each of the 21 profile parameters by taking the columns of the basis variable regression matrix having the 28 highest regression coefficients for that particular parameter and performing a second optimised regression using only these basis variables. Using this procedure, the regression variances for the second-pass 28-variable regression is only a few percent higher than for the first-pass 51-variable regression whereas a single-pass 28-variable regression yields the order of 50% increased variances. The extra online calculations due to this refinement are trivial: for a given equilibrium/raw spectrum, the 51 x 1 vector of linear and quadratic *p.c.* combinations needs to be computed just once. Pointers into this vector select the appropriate 28 elements for each parameter and these are simply multiplied by this parameter's FP coefficients to yield the parameter value.

3.4 The Impact of Errors in the Raw Data. The incorporation into the analysis of the expected error levels in the raw signals merits special attention. In the absence of detailed technical information on the error levels in the magnetic data, an uncertainty of 10% of the rms deviation of the signal value over the equilibrium database was presumed (see [3] also). For the the profile data, the mean values for each channel of the error bars returned by the LASER program were computed from the 2000-spectrum database. Table I lists the results — the 16^{th} channel has been included for completeness. Since the eigenvectors are regarded as inherent quantities determined by the fixed layout of the experiment and the diagnostic equipment, the Principal Component Analysis is performed on the exact simulated raw measurements. For the FP regression, on the other hand, it has been found by experience that more stable results ensue when the raw data is pre-perturbed, or 'conditioned' by a noise level typically one half of that assumed experimentally. This imparted noise will then propagate into *p.c.*'s that are subsequently calculated from the perturbed raw measurements. To use regression coefficients as a measure of correlation between regressed plasma parameters and each basis variable *p.c.* combination, it is useful to scale each of the latter to unit variance.

Together with its natural variance given by its eigenvalue magnitude, each *p.c.* now exhibits an additional noise variance. Hence for a basis variable consisting of a single *p.c.* and allowing for differing error levels for each raw measurement, the following normalisation was employed:

$$b_m = \widehat{x}_i = \frac{x_i}{\sqrt{\lambda_i^2 + \sum_{j=1}^{24} \epsilon_j^2 \cdot w_{ji}^2}} \qquad (2a)$$

where: $\mathbf{q}$ is the measurement vector, $\mathbf{w}$ is the eigenvalue matrix whose i^{th} column is the i^{th} eigenvector, $x_i = \sum_{j=1}^{24} q_j w_{ji}$ is the i^{th} *p.c.* , λ_i^2 is the i^{th} eigenvalue and ϵ_j is the error level for the j^{th} raw measurement. This relation is easily generalised for *p.c.* combinations: For a basis variable made up of a product of two different *p.c.*'s we have:

$$b_m = \widehat{x}_i \cdot \widehat{x}_k \qquad (2b)$$

Finally for a basis variable quadratic in a single *p.c.* we have:

$$b_m = \frac{1}{\sqrt{2}}(\widehat{x}_i^2 - 1.0) \qquad (2c)$$

where the constants in the latter expression were found to give basis variables of approximately zero mean and unit variance. Of the retained *p.c.* combinations, the least significant (smallest λ^2) are most affected by the extra noise variance and any correlations that might have existed between the exact *p.c.*'s and the regressed parameters are consequently degraded. The pruning procedure described in the preceding subsection weeds out just such weakly correlated combinations before yielding the final FP coefficients following the second optimised regression. FP error bars are now calculated by freshly perturbing the original exact simulated raw data with Gaussian noise of the experimentally expected magnitude (generating a new set of exact raw data is unnecessary), recalculating the matrix of *p.c.* combinations and using the calculated FP coefficients to generate a set of recovered dependent variables. These are compared to the exact plasma parameters (the dependent variables that were used in the regression) to determine the error in their recovery. As the uncertainty of near-axis profile values was expected to be an increasing function of $\beta_\mathrm{p} + l_\mathrm{i}/2$, the FP error bars were in turn regressed against the recovered $\beta_\mathrm{p} + l_\mathrm{i}/2$ and the expected variation is confirmed.

4. RESULTS

4.1 FP Results. Figs. 2 and 3 show a typical set of recovered electron temperature and density profiles as a function of normalised geometrically averaged flux surface radius. The FP profile is the imaginary line bisecting the shaded band. The continuous line is explained below. The results of the regression analysis and the method by which they are used to arrive at information such as that displayed in Figs. 2 and 3 are now detailed.

The output of the PCA/FP analysis of the simulated database consists of the following information:

(a) The mean and standard deviation of each of the 24 raw measurements. Real raw measurements (the magnetic data will first have been scaled to unit plasma current) are scaled using these factors as follows: $q_i^{scaled} = (q_i^{raw} - < q_i >)/\sigma_i$.

(b) Maximum and minimum values of each raw measurement. Any real raw measurement lying outside these limits (either it is faulty or there was insufficient variation of operating parameters in generating the database) is flagged, and the *p.c.*'s computed from such a set of measurements should not be considered trustworthy.

(c) The 24 eigenvectors (each with 24 elements) used to compute the *p.c.*'s from a set of real raw measurements scaled as in (a) above.

(d) A pointer array into the 51 *p.c.* combinations selecting the 28-element subset to be used in the recovery of each individual parameter.

(e) The 28 FP regression coefficients for each recovered parameter. The parameter value is obtained by taking the inner product of these coefficients with the subset of *p.c.* combinations selected in (d).

(f) Maximum and minimum values of the recovered parameters. As in the case of an exceptionally valued raw measurement, doubt should be cast on the results when a recovered parameter falls outside these limits.

(g) A set of 4 regression coefficients for each recovered profile value with which its relative error bar is calculated as a cubic polynomial in the recovered value of $\beta_p + l_i/2$.

Using the Table I error levels for the 15 channels and the previously stated 10% level for the 9 magnetic measurements, the resulting FP error bars for three sample values of $\beta_p + l_i/2$ are listed in Table II. Note that the smallest error bars occur in the middle of the profile where most data points lie and where the relative errors for individual channels are also at a minimum (see Figs. 2 and 3 for graphical expression).

The primary check on the recovered profiles is by comparison with plots of the raw points versus flux surface radius which, for ASDEX equilibria, are adequately determined by the shifted flux circles model. It is important to note that these ρ values are

not explicitly involved in the above-described FP regression. The required information is implicitly contained in the 'mixed' eigenvectors/$p.c.$'s referred to in subsection 3.2. There is no reason why they cannot be explicitly recovered, however, and an entirely separate FP regression was performed to recover the geometrically averaged flux surface radii defined as the argument in the RHS of Eq. (1) as well as the quantities previously determined in [3] using the 9 magnetic measurements only. The FP coefficients arising from this regression were incorporated into a separate program, FP2, and on applying this to actual ASDEX dicharges, the FP - recovered flux surface radii are found to be in close agreement with those obtained using the shifted flux circles model, typically differing by a less than 1% (i.e. 4 mm for ASDEX dimensions).

The code FPYAG was written to perform an FP electron temperature and density profile recovery (using CMS-archived ASDEX shot data) for every YAG timepoint satisfying a specified shotnumber and time window. A users guide is provided in the appendix. The output (FP2 is used for the flux radii results) includes tables of raw temperatures and densities with corresponding fractional error bars (as returned by the LASER program), normalised flux radii calculated by (a) FP (b) The shifted flux circles model and finally the 21 - point recovered temperature and density profiles with FP - calculated error bars. A plot program, FPYPL, allows graphical representation of various combinations of the output data. In addition, this code (whose operation is also described in the appendix) performs a truncated Gaussian-like fit to the raw profile data using either the FP or shifted flux circles ρ values (they both give virtually the same fit parameters). Like the spline profiles used to generate simulated raw data for the FP regression, this fitting model, which is frequently used to summarise the Thompson scattering profiles, has four free parameters. The profile fitted in this manner:

$$P(\rho) = Ge^{-\{A\rho^2+B\rho^4+C\rho^6\}} \tag{3}$$

where G,A,B and C are least squares fitted parameters and $P = T_e$ or $P = n_e$, is graphically compared to the FP result. For discharges in the ohmic phase, where the magnetic axis is close to the R position of the vertical laser chord (163 cm), the FP and truncated Gaussian (TG) fits agree closely (see Fig. 2). For a laser chord - magnetic axis separation of about 15 cm, however, the extrapolated axis temperatures may differ by the order of 30% between the two fits (see Fig. 4).

4.2 Comparison with ECE axis temperatures. Independent diagnostic information is required if we are to resolve the question as to which, if any, of the two fits described in the preceding subsection give realistic axis temperatures. Such information

is available from the electron cyclotron emission (ECE) diagnostic which offers electron temperature time profiles (millisecond resolution) from 7 cm - wide scattering volumes centred on four selectable positions along a major radius in the horizontal mid-plane. The incorporation of the ECE measurements themselves into the FP analysis would be difficult on account of the variable spatial positioning of the channels, but reliance on the YAG temperatures alone is also motivated by the fact that the YAG diagnostic is valid over a wider range of plasma parameters than ECE; the latter, in particular, being limited by high densities and low toroidal magnetic fields. The discharges cited below had favourable parameters for both diagnostics and, more to the point, the four ECE channels were well positioned to follow the excursions of the magnetic axis, and hence reliable axis temperatures could be obtained from a parabolic fit (of temperature versus flux radius) through the four channels. In the ohmic phase, the magnetic axis lies relatively close to the laser path and axis quantities may be reliably estimated from the YAG data alone. When ohmic YAG axis temperatures are compared with those from ECE, however, it is found that for a given discharge the ratio $r = T_{YAG}/T_{ECE}$, though consistent, may lie anywhere in the range $1.0 \leq r \leq 1.25$. The resolution of this discrepancy is outside the ambit of the present work. The temporal behaviour of the axis temperature as given by (a) ECE (scaled), (b) FP and (c) TG fits is graphically presented for two ASDEX discharges, both with additional heating power from neutral beams.

In shot # 19151 ($I_p = 280kA$, $B_t = 2.4\ T$, $n_{el} = 2.7 \cdot 10^{13}\ cm^{-3}$, see Fig. 5) 0.5, 1 and 2 MW of beam power were consecutively applied in a discharge where the H regime was not reached. In the three ohmic phases, where $R_{axis} - R_{laser} \leq 7$ cm, all three fits agree fairly well. For the three NBI phases, however, while the FP axis temperature continues, with only a few exceptional points, to stay very close to the reliable ECE curve, the TG points become progressively more erratic with increasing remoteness of the laser position from the magnetic axis. Note that the FP - ECE agreement continues to be very good as $R_{axis} - R_{laser}$ retreats from its high of 12 cm after the beams are turned off at 1.8 seconds.

In shot # 16981 ($I_p = 310kA$, $B_t = 2.6\ T$, $n_{el} = 3.4 \cdot 10^{13}\ cm^{-3}$, see Fig. 6) 2.5 MW of beam power were applied between 1.1 and 1.5 seconds. The L to H transition occurred at 1.27 seconds and the characteristic spikes in the H_α trace lasted until 1.58 seconds, some 80 ms after the beams were switched off. The H_α intensity abruptly increased at 1.4 seconds, however, signifying a deterioration in confinement, though the level remained well below that of the L phase. During the period of improving or flat confinement (up to 1.4 seconds), FP axis temperatures are considerably less erratic and much closer to the ECE values than the TG - fitted values despite the large

$R_{axis} - R_{laser}$ attained (up to 15 cm). After the deterioration at 1.4 seconds, however, a marked discrepancy develops between FP and ECE (similarly for TG, though the latter's points are more scattered as usual) and it remains until the H to L transition at 1.58 seconds. This disagreement, observed in a number of similarly analysed discharges with an abrupt deterioration in confinement during the H phase, arises following the deterioration because the ECE temperature profile appears to peak at an R value well outside the magnetic axis position as given by external magnetic measurements.

5. Discussion

The following points should be noted:

1) A problem arises in the case of strongly positive z_{axis} if the separatrix lies above the bottommost channel (# 15). Ideally, a separate FP regression should be performed in which the 15^{th} channel is not utilised. A preliminary check on the separatrix position would then be required to determine whether the 15-channel or 14-channel set of FP coefficients is appropriate. Because of the relatively high error level in channel 15 (and hence the low information content) it was deemed sufficient in the present work to set the value of any channel lying outside the separatrix equal to the value of the last point lying inside. This procedure was applied both to the simulation and to the on-line evaluation stages. For positive z_{axis} equilibria, this somewhat reduces the steepness of the recovered profile in the separatrix region. This is not a cause for concern, however, since the normal correspondence of channel 15 to a flux surface radius (normalised) of about 0.9 means that that portion of the recovered profile lying between 0.9 and 1.0 (the separatrix) is unreliable anyway.

2) Despite the assumption of shifted flux circles in generating the spline database (this could, in fact, have been circumvented by producing the FP2 program in the first instance), the simulated profile raw data were generated using only the cross-sectional area of the flux surface intersecting each channel without any assumptions about the flux surface geometry. The technique, in other words, is not restricted to ASDEX equilibria; on the contrary, it can be readily applied to the more complicated geometries that will be typical of ASDEX-UPGRADE.

3) Time precluded a comparison of recovered electron density profiles with line density data, so they cannot be considered to be as well validated as the temperature profiles. It is planned, however, to combine data from YAG and the 4-channel HCN-laser interferometer; whose fixed geometry, in contrast to the variable positions of the 4 ECE channels, make it a further candidate-diagnostic for FP.

4) The online FP calculation routine requires *c.* 5 kilowords of storage and requires *c.* 3500 floating point operations (flops) per entire profile. At a by no means exceptional computation speed of 5 Mflops s^{-1} this implies a 0.7 msec calculation on a dedicated microprocessor. Though the profile recovery calculation using FP coefficients is consequently extremely rapid, the focus of the present work is to demonstrate the ability of FP to combine physically dissimilar data from separate diagnostics. The spatial temperatures and densities are certainly not primitive diagnostic signals, and it would require

inclusion of the latter quantities in place of the presently used YAG data to strictly demonstrate that profile information from this diagnostic can be provided within a time frame compatible with the requirements for a possible real-time control application.

ACKNOWLEDGEMENTS

The author is grateful to K. Lackner for providing direction, O. Gruber for helpful discussions, and H. Murmann and A. Eberhagen for making available data from the YAG and ECE diagnostics, respectively. Technical assistance was rendered by E. Sombach. Lastly, the generous assistance of B.J. Braams in familiarising us with the PCA/FP approach to plasma parameter evaluation is warmly acknowledged. This work was performed under the Euratom - IPP and Euratom - UCC association agreements.

References

1. Wind, H., in "Proceedings of the 1972 CERN Computing and Data Processing School", CERN 72–21, 1972, pp. 53–106.
2. Wind, H., (a) *Principal Component Analysis and its Application to Track Finding,* (b) *Interpolation and Function Representation*, in "Formulae and Methods in Experimental Data Evaluation", Vol. 3, European Physical Society, Geneva, 1982.
3. Braams, B.J., Jilge, W. and Lackner, K., *Fast determination of plasma parameters by function parametrization*, Nucl. Fusion **26** (1986), 699–708.
4. Braams, B.J. and Lackner, K., *A Proposed Method for Fast Determination of Plasma Parameters*, Report IPP 1/228, Max-Planck-Institut für Plasmaphysik, 1984.
5. Röhr, H., Steuer, K.-H., Schramm, G., Hirsch, K., and Salzmann, H., *First high-repetition-rate Thomson scattering for fusion plasmas*, Nucl. Fusion **22** (1982), 1099–1102.
6. Meisel, D., Murmann, H., Röhr, H., Steuer, K.-H. and the ASDEX-TEAM, *Periodic Thompson scattering diagnostic with 16 spatial channels on ASDEX* (13^{th} European Conference on Controlled Fusion and Plasma Physics, Scliersee, April 1986), Europhysics Conference Abstracts **10c-I** (1986), 97–100.
7. Lackner, K., *Computation of Ideal MHD Equilibria*, Comput. Phys. Commun. **12** (1976), 33–44.
8. Mardia, K.V., Kent, J.T. and Bibby, J.M., "Multivariate Analysis", Academic Press, London, 1979.
9. Montgomery, D.C. and Peck, E.A., "Introduction to Linear Regression Analysis", Wiley, New York, 1982.
10. Draper, N.R., and Smith, H., "Applied Regression Analysis", 2nd Ed., Wiley, New York, 1981.

TABLE I

R-position for all channels: 163 cm.

channel #	z-position (cm)	$\overline{\frac{\delta n_e}{n_e}}$	$\overline{\frac{\delta T_e}{T_e}}$
1	20.0	.08	.19
2	16.5	.04	.07
3	12.7	.03	.07
4	8.2	.03	.06
5	4.6	.03	.06
6	0.0	.03	.10
7	−3.6	.03	.06
8	−7.2	.02	.05
9	−11.2	.03	.06
10	−15.5	.04	.08
11	−19.0	.09	.13
12	−23.0	.17	.17
13	−27.0	.06	.13
14	−31.2	.13	.22
15	−35.3	.24	.30
16	−39.4	1.11	.92

TABLE II

ρ	$\langle \delta T_e(\rho)/T_e(\rho) \rangle$ $(\beta_p + l_i/2 = 0.75)$	$\langle \delta T_e(\rho)/T_e(\rho) \rangle$ $(\beta_p + l_i/2 = 2.00)$	$\langle \delta T_e(\rho)/T_e(\rho) \rangle$ $(\beta_p + l_i/2 = 4.00)$
0.00	.030	.038	.137
0.05	.030	.038	.135
0.10	.029	.036	.130
0.15	.026	.033	.123
0.20	.023	.029	.112
0.25	.021	.025	.098
0.30	.018	.021	.080
0.35	.018	.018	.059
0.40	.020	.018	.042
0.45	.022	.022	.031
0.50	.025	.026	.028
0.55	.027	.028	.029
0.60	.028	.028	.029
0.65	.031	.030	.029
0.70	.038	.036	.034
0.75	.047	.044	.047
0.80	.058	.055	.065
0.85	.081	.079	.088
0.90	.132	.130	.122
0.95	.256	.247	.236
1.00	.555	.543	.493

APPENDIX

The following files should be copied from userid PJM :

RY	EXEC
FPYAG	TEXT
FP2YAGV	TEXT
FP2V	TEXT
FP2PCAV	TEXT
FPYAGPCA	TEXT
RYPL	EXEC
FPYPL	TEXT

Your Virtual Machine, which must have access to the ASDEX data disks, requires 3 megabytes of storage. The CMS command is DEF STOR 3M . After the disabled wait message, enter I CMSL . LINKNAG may also be necessary to link to the Nag libraries. Check, using the SHOTS utility, that any shots you may wish to analyse are online. Enter RY to run FPYAG. Enter shotnumber, start time, finish time (both in seconds) and skip factor. The latter quantity when set to 'I' causes every I^{th} spectrum-pair to be processed. Set it to 1 to process every YAG time-point inside the time window. When the analysis is finished, you may proceed to enter further shotnumbers and time windows. To terminate the session, enter shotnumber $= -100$ (plus any old time window and skip factor) and the code exits. Three results files are created or overwritten each time FPYAG is executed. Their names and formats are as follows:

FILE FT12F001 has a 13-line entry for each YAG timepoint. Line 1 contains the following eight fields:

SHOT # Time R_{axis} R_{geom} Z_{axis} Z_{geom} $\sqrt{\frac{A_P}{\pi}}$ $\beta_p + l_i/2$

where A_P is the plasma area and $\sqrt{\frac{A_P}{\pi}}$ is the geometrically averaged plasma minor radius. Lines 2-4 contain the raw temperatures for channels 1-15 as listed in Table I. Lines 5-7 contain the experimentally derived relative errors for each channel. Lines 8-13 contain the density data corresponding to the temperature data in lines 2-7. Temperatures are in eV; densities are in units of $10^{11} cm^{-3}$.

FILE FT11F001 has a 22-line entry for each YAG time-point. Lines 1-4 contain the 21 FP-recovered temperatures for the normalised flux surface radius sequence: 1.0, .95, .9, ... , .05, 0.0 . Lines 5-8 contain the corresponding FP relative error bars. Lines 9-16 contain the density results and follow the same format as lines 1-8. Lines 17-19 contain the FP-recovered normalised flux surface radii for channels 1-15. Lines 20-22

contain the shifted flux circles - calculated radii. Temperature and density units are the same as in file FILE FT12F001.

FILE FT17F001 contains two lines of summary information for each time-point. Line 1 has the following fields:

SHOT # Time $\beta_p + l_i/2$ χ^2 T_{axis}(FP) δT_{axis}(FP)/T_{axis}(FP)

where $\chi^2 = \sum_{i=1}^{24} \hat{x}_i^2$ ($\hat{x}_i$ is defined in Eq. (2a)). χ^2 should normally have a value of about 24, although the variable magnitude of the experimental YAG error bars will occasionally produce a value as high as 100. Inspection of the graphical results is mandatory in such cases. Line 2 has the corresponding information for the density results. The units are the same as in the other two files.

The user may write his own software to plot these results, but the code FPYPL may be used to produce output like that presented in Figs. 2 to 4. FPYPL uses the current FT11F001 and FT12F001 results files. Start by entering RYPL. Enter 11 for Fig. 2 or Fig. 3 type output, or 12 to get spatial plots of the raw data. Next enter -5 for a plot or 0 to skip the current timepoint. If a plot is selected, enter 1 for temperature or 2 for density. Each timepoint is processed in sequence until -100 is entered as the plot option, whereupon FPYPL exits. Finally enter DOPLOT FPY PL (PLOTLG6 to direct the contents of the plot file FPY PL to the laser graphics device.

FIGURE CAPTIONS

Fig. 1. Poloidal cross-section of the ASDEX experiment showing flux surfaces, multipole shaping coils and raw measurement geometry. $\psi_3 - \psi_1$, $\psi_4 - \psi_2$ and $\psi_3 - \psi_4$ are the poloidal flux differences used. B_1 to B_4 are the poloidal field measurements. The principal multipole current, I_{mpc}, flows through the two bigger multipole shaping coils marked with the symbol $+$. The magnitude of the return current through the four smaller coils is normally $\frac{1}{2} I_{mpc}$ but is reduced by an amount proportional to the magnitude of the MPIS signal when the latter quantity is non-zero. The vertical line with 16 crosses represents the scattering centres along the YAG laser chord. The co-ordinates are listed in Table I.

Fig. 2. T_e in eV versus normalised flux surface radius. The individual points points are the raw data with experimentally determined error bars. The full line is the fit in Eq. (3) and the fitted parameters are tabulated as G,A,B and C. The 21 FP profile points are linked smoothly by the plotting software and the FP error bars are represented by a shaded band whose vertical width is two standard deviations as calculated by FP. The profile, which was omitted for clarity, bisects the shaded area. The FP axis temperature is tabulated as T0. This spectrum lies in the ohmic phase of the discharge.

Fig. 3. n_e in units of $10^{14} cm^{-3}$ versus normalised flux surface radius. The FP axis density is tabulated as N0. The individual plots have the same significance as in Fig. 2.

Fig. 4. This spectrum lies in the H phase of this discharge. The individual plots have the same significance as in Fig. 2.

Fig. 5. Shot # 19151: $T_e(axis)$ versus time for ECE, FP and the truncated Gaussian fit (see Eq. (3) in the text). The ECE data is scaled to agree with FP in the the ohmic phase. The more lightly dashed curve is R_{axis} from the FP2 program.

Fig. 6. Same as Fig. 5, but for shot # 16981.

Fig 1

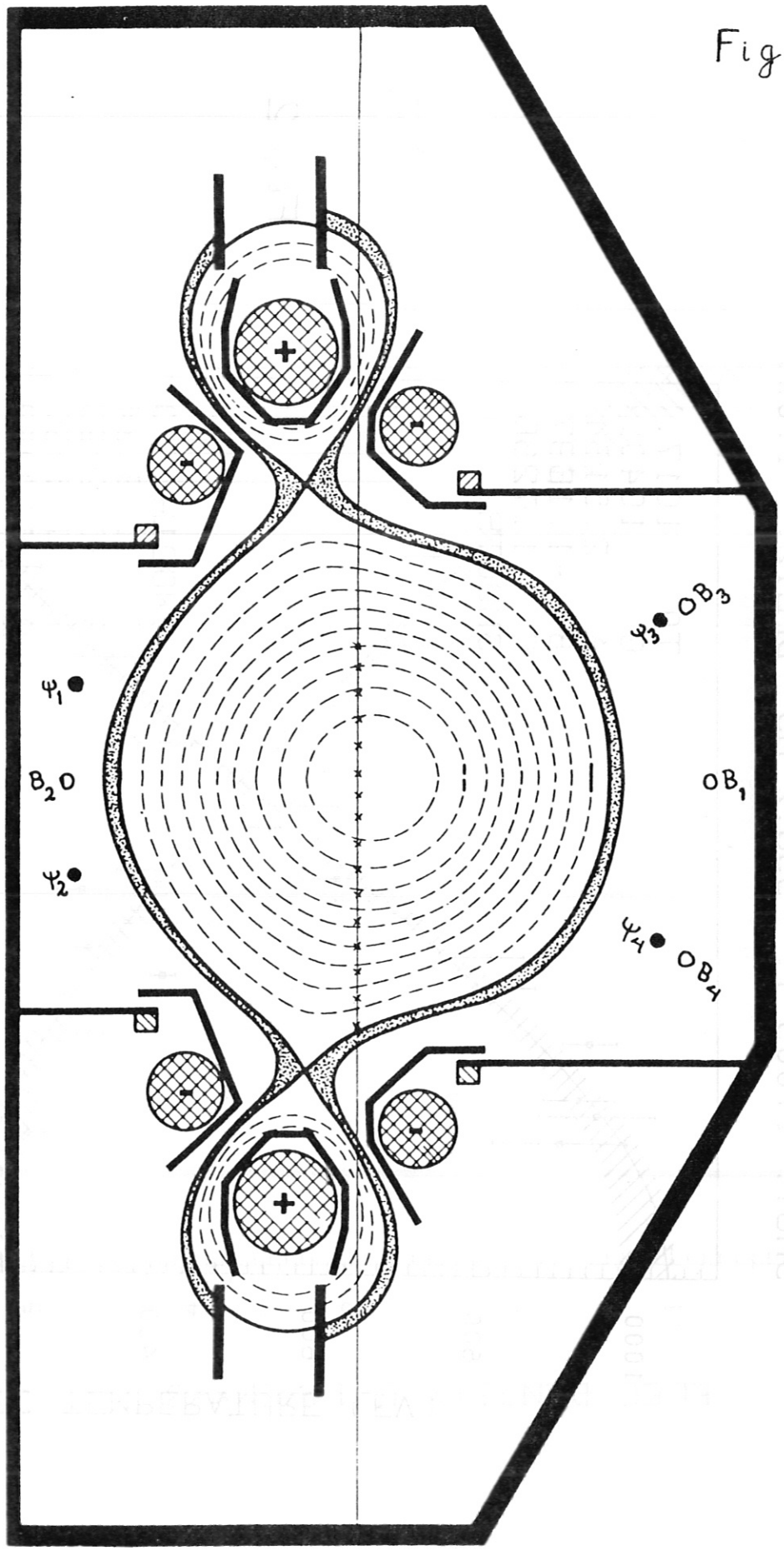

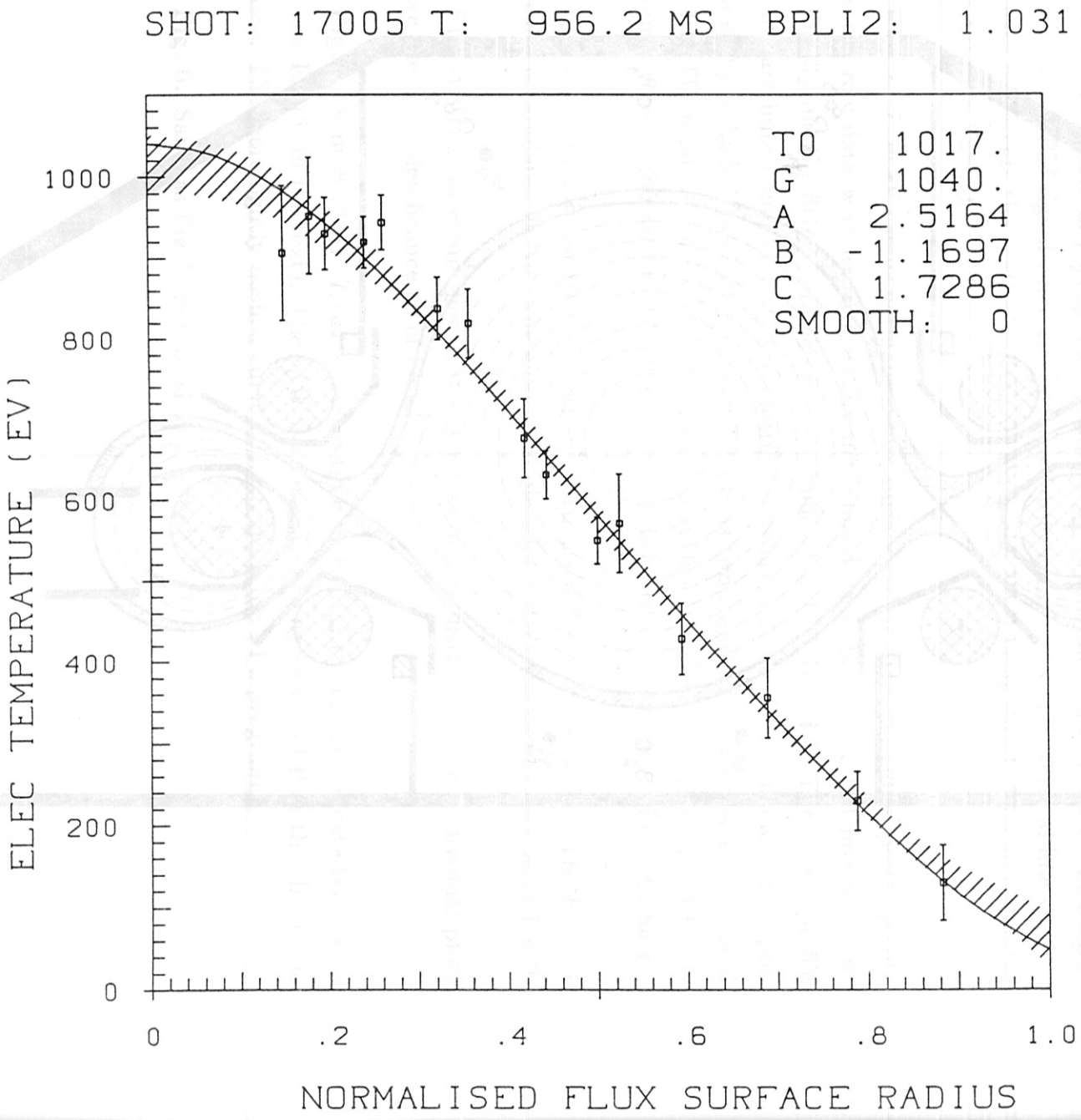
SHOT: 17005 T: 956.2 MS BPLI2: 1.031
TO 1017.
G 1040.
A 2.5164
B -1.1697
C 1.7286
SMOOTH: 0
ELEC TEMPERATURE (EV)
1000
800
600
400
200
0
0
.2
.4
.6
.8
1.0
NORMALISED FLUX SURFACE RADIUS

Fig 2

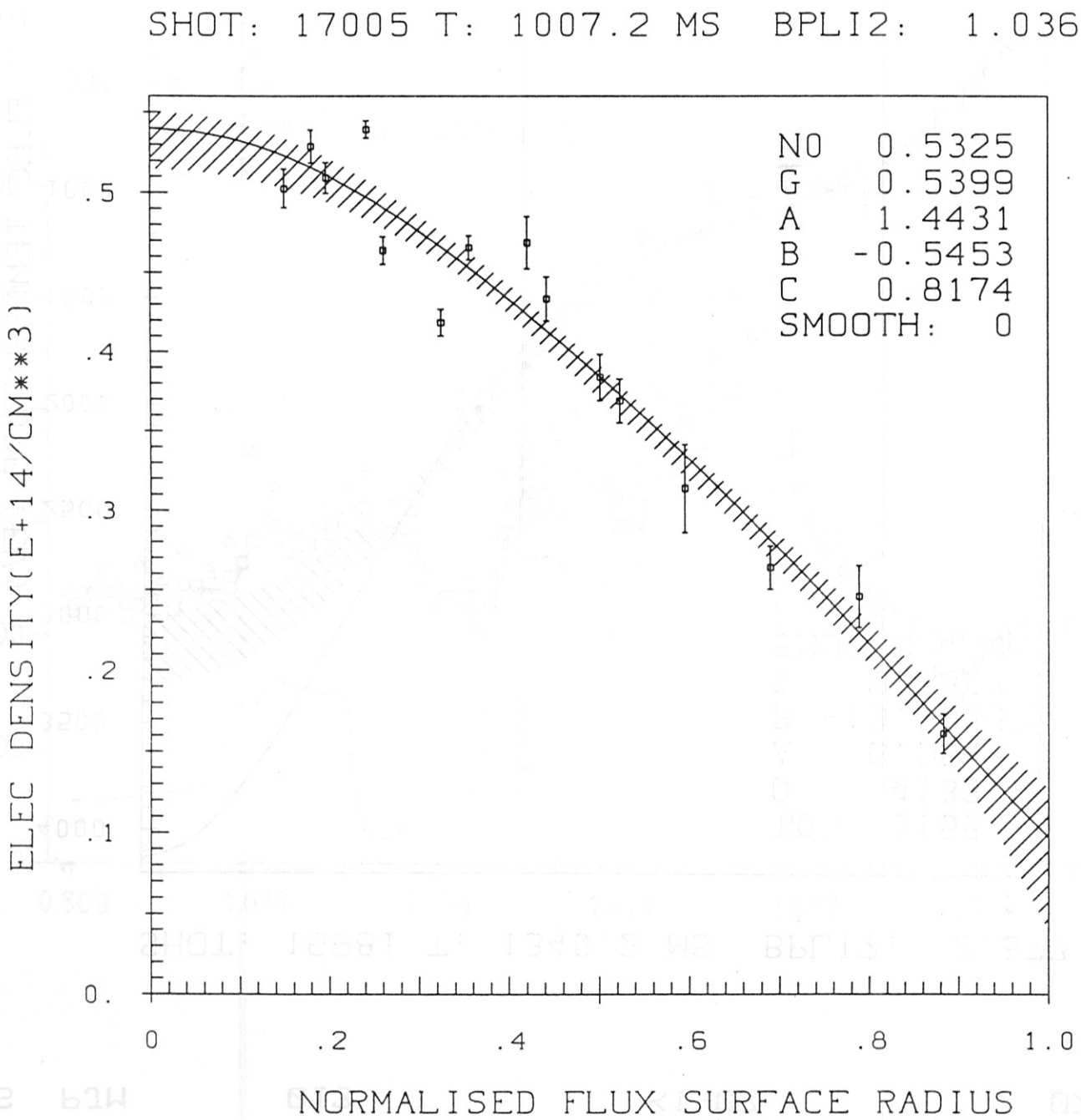
SHOT: 17005 T: 1007.2 MS BPLI2: 1.036
NO 0.5325
G 0.5399
A 1.4431
B -0.5453
C 0.8174
SMOOTH: 0
ELEC DENSITY(E+14/CM**3)
0.
.1
.2
.3
.4
.5
0
.2
.4
.6
.8
1.0
NORMALISED FLUX SURFACE RADIUS

Fig 3

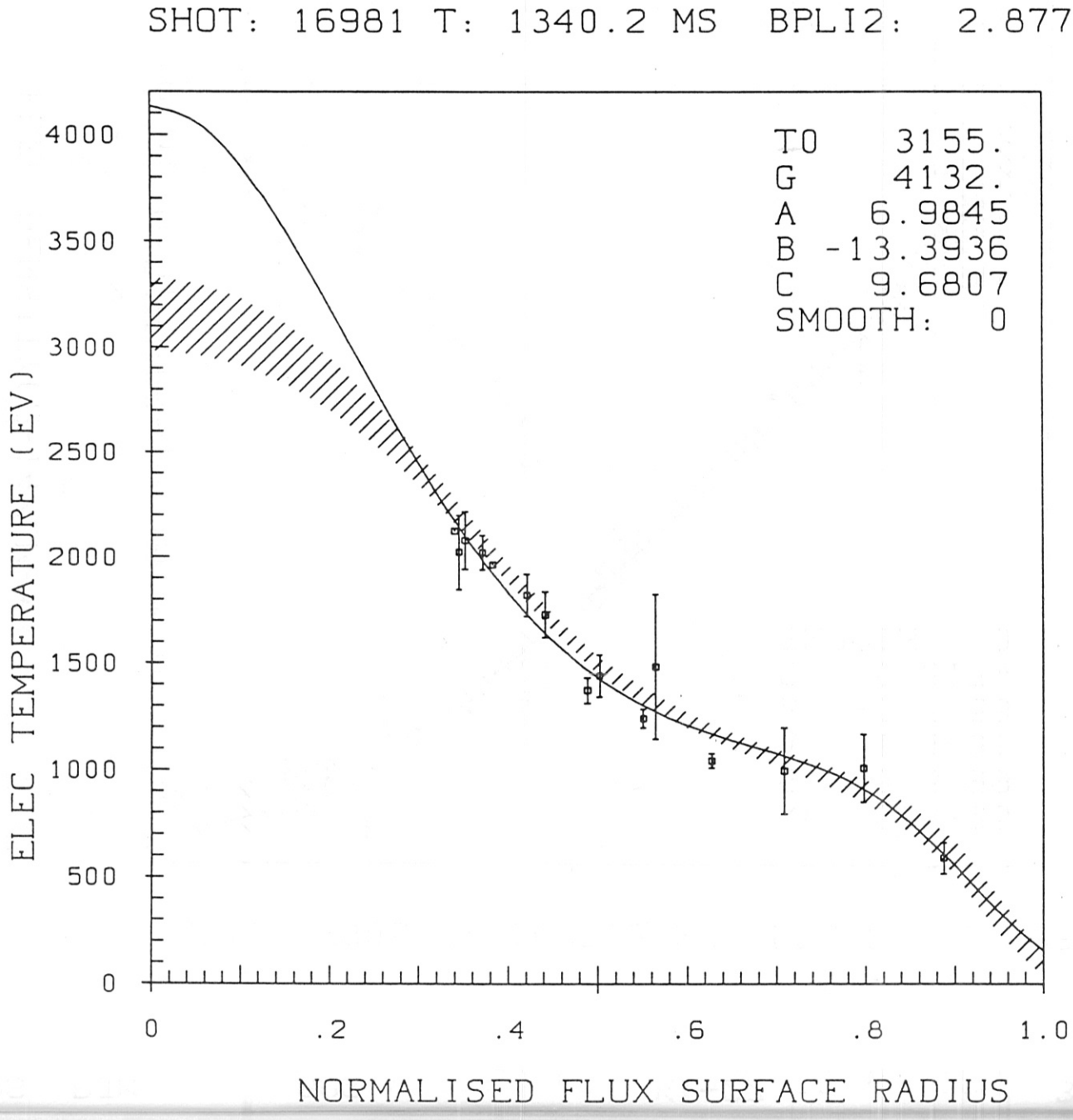
SHOT: 16981 T: 1340.2 MS BPLI2: 2.877
T0 3155.
G 4132.
A 6.9845
B -13.3936
C 9.6807
SMOOTH: 0
ELEC TEMPERATURE (EV)
4000
3500
3000
2500
2000
1500
1000
500
0
0
.2
.4
.6
.8
1.0
NORMALISED FLUX SURFACE RADIUS

Fig 4

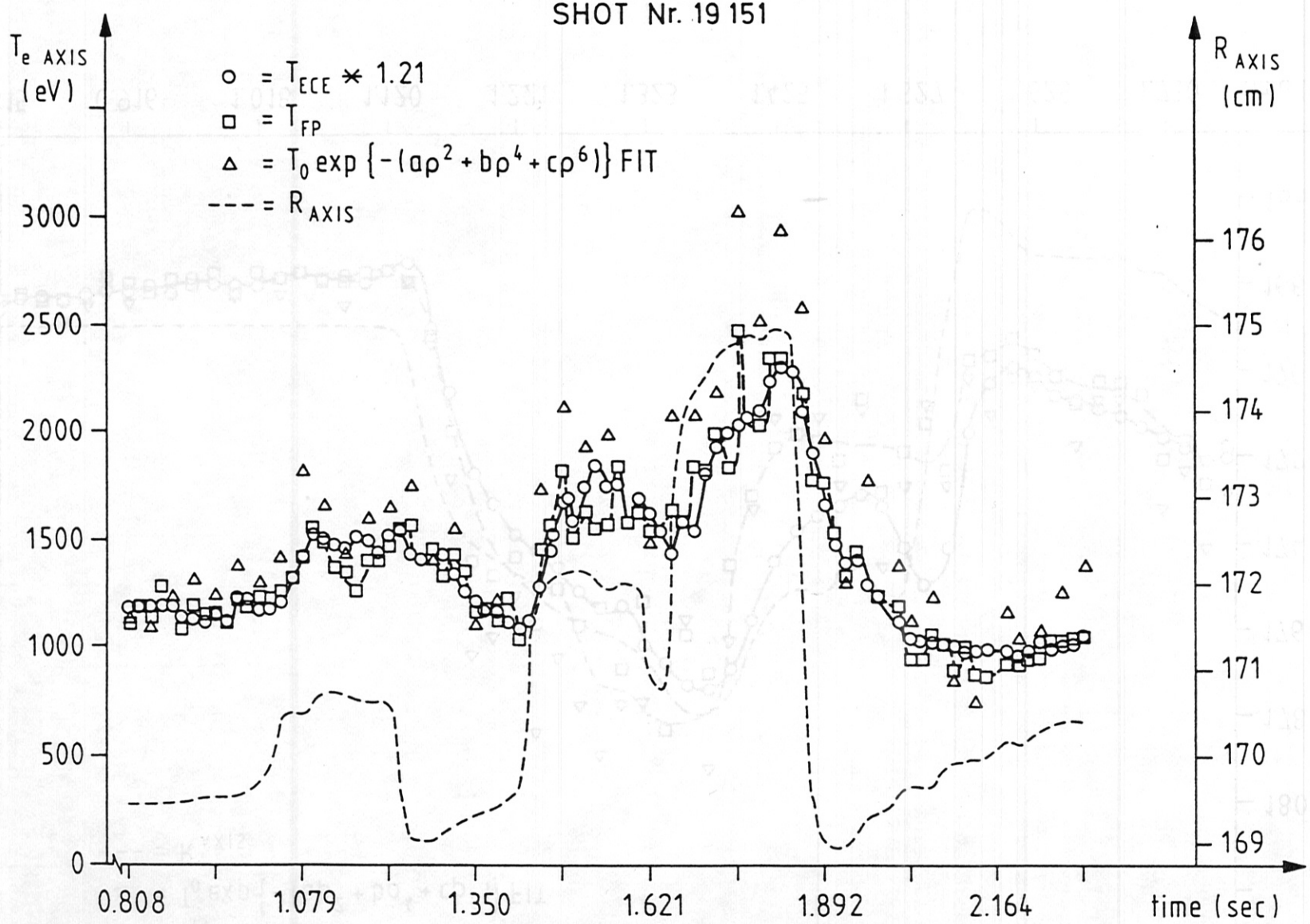
SHOT Nr. 19 151
$T_{e\ AXIS}$ (eV)
R_{AXIS} (cm)
○ = $T_{ECE} * 1.21$
□ = T_{FP}
△ = $T_0 \exp\{-(a\rho^2 + b\rho^4 + c\rho^6)\}$ FIT
--- = R_{AXIS}
3000
2500
2000
1500
1000
500
0
176
175
174
173
172
171
170
169
0.808
1.079
1.350
1.621
1.892
2.164
time (sec)

Fig 5

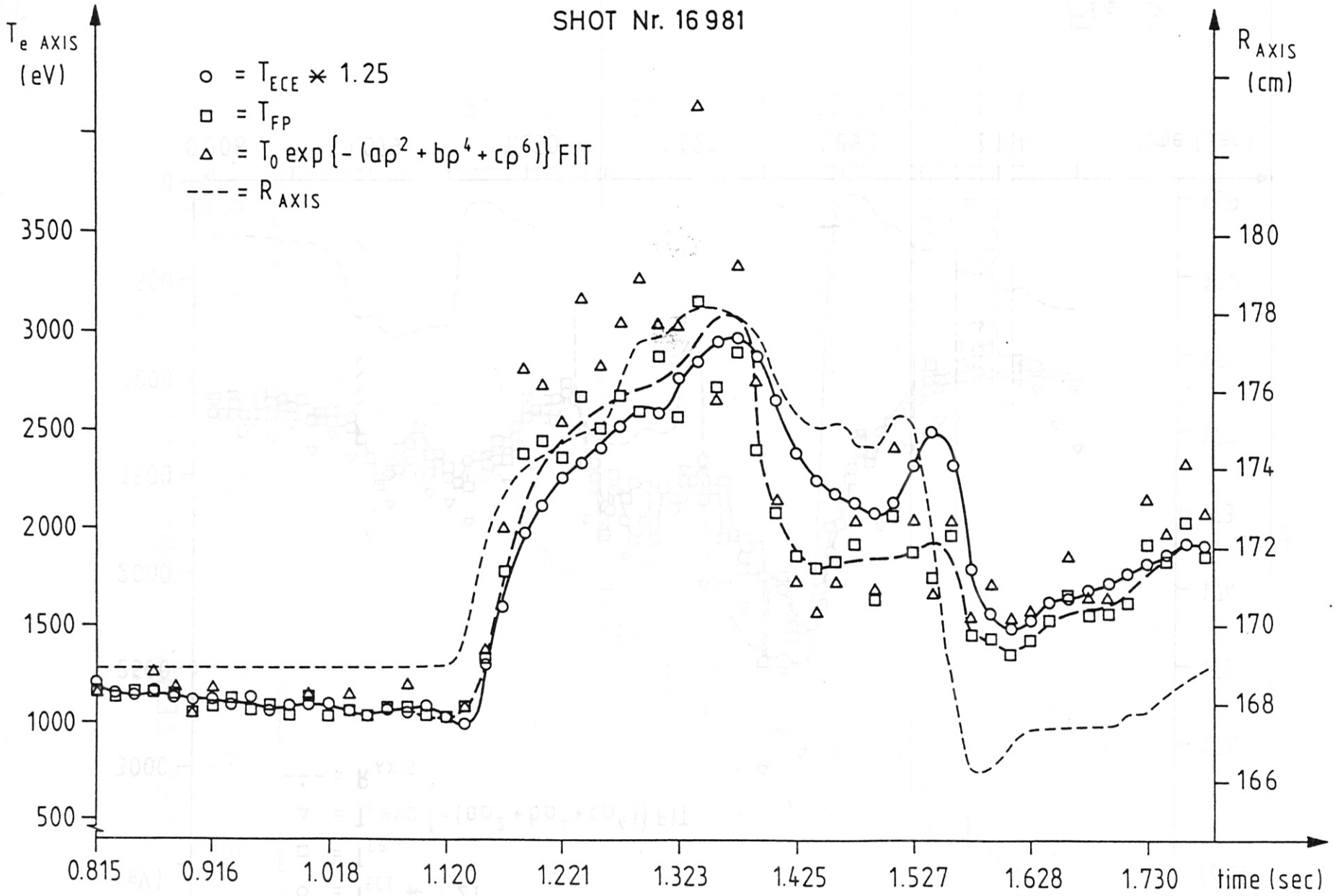
SHOT Nr. 16 981
$T_{e\ AXIS}$ (eV)
R_{AXIS} (cm)
○ = $T_{ECE} * 1.25$
□ = T_{FP}
△ = $T_0 \exp\{-(a\rho^2 + b\rho^4 + c\rho^6)\}$ FIT
--- = R_{AXIS}
3500
3000
2500
2000
1500
1000
500
180
178
176
174
172
170
168
166
0.815
0.916
1.018
1.120
1.221
1.323
1.425
1.527
1.628
1.730
time (sec)

Fig 6